Closed-Chain Hand Exoskeleton Digital Twin in ROS 2 with Constraint-Consistent Reduced Dynamics

Amelia Gioscia[1], Marcello Bari[1], Paolo Lino[1], Stefano Mazzoleni[1,2,3], and Marina Cosmo[1]

Abstract— **Hand exoskeletons are increasingly used in robot-assisted rehabilitation to support motor recovery and enable task-oriented therapy. Accurate digital representations of these devices are essential for simulation, monitoring, and model-based control. However, many rehabilitation mechanisms involve closed kinematic chains, while common robotics modeling frameworks such as URDF rely on tree-structured representations that do not directly support kinematic loops. This work presents a constraint-consistent digital twin of a prototype hand exoskeleton implemented within a ROS 2 framework. The mechanical architecture is derived from a CAD model and converted into a URDF representation. Loop-closure constraints are reconstructed numerically through nonlinear optimization, enabling simulation of the closed-chain mechanism using standard rigid-body dynamics tools. The constrained multibody dynamics are projected onto the null space of the constraint Jacobian, yielding a reduced nonlinear dynamic model with a single independent coordinate. Preliminary simulations demonstrate the numerical stability of the framework and the accurate reconstruction of the kinematic constraints. Hardware torque–position measurements are currently being performed, and datasets are being acquired to identify real system parameters, calibrate the digital twin, and assess its predictive accuracy under representative actuation profiles, enabling subsequent real-time model-based control development.**

I. INTRODUCTION

Robot-assisted rehabilitation has become an important tool for supporting motor recovery after neurological injuries [1]. Robotic devices enable repetitive and controlled movements while providing assistance and monitoring during therapy sessions. In particular, hand exoskeletons have been widely investigated for upper-limb rehabilitation tasks such as grasping and finger motion. Several control strategies have been proposed to improve human–robot interaction, including approaches designed for virtual-reality-based rehabilitation tasks [2]. In parallel, the Digital Twin paradigm has emerged as a framework for representing physical systems through computational models capable of monitoring and predicting their behavior [3]. More recently, this concept has been extended to healthcare through Human Digital Twins, which integrate sensing data and computational models to represent both patient and device behavior in rehabilitation scenarios [4]. Despite these advances, constructing accurate digital models of rehabilitation devices remains challenging. Many exoskeleton mechanisms involve closed kinematic chains, whose accurate modeling requires dedicated constraint-handling formulations that are not straightforwardly supported by standard robotics frameworks. Since commonly used formats such as URDF assume tree-structured kinematic models, representing closed-chain mechanisms while preserving dynamic consistency remains an open challenge. To address this issue, this work proposes a constraint-consistent digital twin of a hand exoskeleton prototype implemented within a ROS 2 framework. The mechanical system is derived from a CAD model and represented in URDF, while loop-closure constraints are reconstructed numerically through nonlinear optimization. The constrained multibody dynamics are projected onto the null space of the constraint Jacobian, yielding a reduced nonlinear dynamic model suitable for simulation and analysis. From a clinical perspective, the proposed Digital Twin could also support subject-specific rehabilitation planning by enabling virtual pre-configuration of the hand exoskeleton according to patient-specific anthropometric and biomechanical characteristics prior to therapy sessions. This may help clinicians estimate feasible ranges of motion and personalized assistance settings before physical interaction with the device. In the specific context of finger rehabilitation, where inter-subject anatomical variability is particularly significant, such capability could improve both the clinical appropriateness and the operational efficiency of therapy sessions. The main contributions of this work are: (i) the development of a ROS 2 digital twin of a hand exoskeleton with constraint-consistent dynamics; (ii) a CAD-to-URDF modeling pipeline compatible with standard robotics frameworks; (iii) a numerical method for reconstructing loop-closure constraints; and (iv) a reduced dynamic formulation obtained through null-space projection of the constrained multibody system.

II. MECHANICAL ARCHITECTURE AND URDF REPRESENTATION

The mechanical architecture of the exoskeleton follows the design presented in [5] and consists of a transmission mechanism driving a finger module through a closed-chain linkage. The components were modeled in CAD using a parametric approach to preserve geometric consistency. The assembled mechanism was converted to a URDF model using the ACDCRobot plug-in [6] and integrated within a ROS 2 simulation framework. Since URDF supports only tree-structured kinematic models, selected revolute joints were

[1]The authors are with the Department of Electrical and Information Engineering, Politecnico di Bari, Bari, Italy a.gioscia@phd.poliba.it, m.cosmo@phd.poliba.it, m.bari@studenti.poliba.it, stefano.mazzoleni@poliba.it, paolo.lino@poliba.it

[2]The author is with IMT School for Advanced Studies Lucca, Lucca, Italy. stefano.mazzoleni@imtlucca.it

[3]The author is with the BioRobotics Institute, Scuola Superiore Sant'Anna, Pisa, Italy. stefano.mazzoleni@santannapisa.it

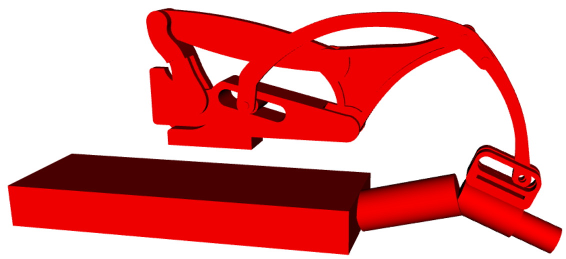

Fig. 1. URDF representation of the hand exoskeleton mechanism.

opened to obtain an equivalent open-chain representation. Loop-closure constraints are not enforced at the URDF level. Instead, auxiliary reference frame pairs are introduced at the opened joints, and their spatial coincidence is imposed numerically during simulation. The reconstructed kinematic behavior and reachable range of motion are qualitatively consistent with the mechanism operation reported in [5], confirming that the CAD-URDF conversion preserves the intended transmission geometry.

III. Kinematic Modeling

The kinematic model of the exoskeleton is computed using the Pinocchio library [7], which provides efficient forward kinematics and Jacobian evaluation from the URDF model. Due to the intentional opening of the kinematic loops, standard forward kinematics does not satisfy the closure conditions. Let $\Phi(q) = 0$ denote the holonomic constraints associated with the coincidence of auxiliary frame pairs. The loop-closure problem is formulated as a nonlinear least-squares optimization. For a fixed crank angle, a subset of joint variables is adjusted to minimize the norm of the constraint residual vector. A trust-region reflective solver with bounded variables is employed and warm-started from the previous configuration to ensure motion continuity. The solution is accepted only if the residual norm falls below a predefined tolerance, ensuring consistency with the original closed-chain mechanism.

A warm-start strategy based on the previously accepted configuration was adopted to improve convergence continuity across the workspace, while bounded optimization variables prevented exploration of kinematically inadmissible configurations.

IV. Constrained Multibody Dynamics

Let $q \in \mathbb{R}^n$ denote the vector of generalized coordinates. The unconstrained joint-space dynamics is

$$M(q)\ddot{q} + h(q, \dot{q}) = \tau \tag{1}$$

where $M(q)$ is the inertia matrix, $h(q, \dot{q})$ collects Coriolis, centrifugal and gravitational effects, and τ is the vector of generalized forces. Due to the closed kinematic chains, the coordinates are not independent and must satisfy the holonomic constraints

$$\Phi(q) = 0 \tag{2}$$

where $\Phi : \mathbb{R}^n \to \mathbb{R}^m$ represents the loop-closure conditions. Introducing Lagrange multipliers $\lambda \in \mathbb{R}^m$, the constrained dynamics becomes

$$M(q)\ddot{q} + h(q, \dot{q}) = \tau + J^T(q)\lambda \tag{3}$$

where the constraint Jacobian is

$$J(q) = \frac{\partial \Phi(q)}{\partial q}. \tag{4}$$

Equations (3) and (2) form a differential–algebraic system. However, the transmission mechanism has only one independent degree of freedom. This property enables the reduction of the constrained multibody dynamics to a scalar nonlinear equation, as described in the next section.

V. Reduction to a 1-DOF Dynamic Model

A. Selection of the Independent Coordinate

The multibody system described by the URDF model is subject to holonomic closure constraints. Although the generalized coordinate vector $\mathbf{q} \in \mathbb{R}^n$ contains multiple joint variables, the transmission mechanism possesses only one independent degree of freedom. The configuration of the mechanism is uniquely determined by the crank joint. Let

$$\theta := q_{crank} \tag{5}$$

denote the crank angle. The remaining coordinates are implicitly determined by the closure constraints.

$$\Phi(q) = 0 \tag{6}$$

Therefore the full coordinate vector can be expressed as

$$q = q(\theta), \tag{7}$$

where the mapping is defined implicitly by the constraint equations.

B. Velocity-Level Constraint Reduction

Differentiating the holonomic constraints $\Phi(\mathbf{q}(\theta)) = \mathbf{0}$ yields the velocity-level constraint

$$J(q)\,\dot{q} = 0, \tag{8}$$

where $J(q) = \partial\Phi(q)/\partial q$ is the constraint Jacobian. Since the mechanism has one degree of freedom, the generalized velocity lies in the null space of $J(q)$ and can be written as

$$\dot{q} = B(q)\,\dot{\theta}, \tag{9}$$

where

$$B(q) = \frac{\partial q}{\partial \theta} \tag{10}$$

represents the admissible motion direction. Differentiating once more gives

$$\ddot{q} = B(q)\,\ddot{\theta} + \dot{B}(q)\,\dot{\theta}. \tag{11}$$

C. Projection of the Full Dynamics

Starting from the constrained dynamics

$$M(q)\ddot{q} + h(q,\dot{q}) = \tau + J^T(q)\,\lambda, \tag{12}$$

the constraint forces are eliminated by projecting onto the null space of the constraint Jacobian. Pre-multiplying by $B^T(q)$ gives

$$B^T M(q)\ddot{q} + B^T h(q,\dot{q}) = B^T\tau, \tag{13}$$

since $J(q)B(q) = 0$. Substituting the kinematic relations from (9) and (11) yields

$$B^T M(q)\big[B(q)\,\ddot{\theta} + \dot{B}(q)\,\dot{\theta}\big] + B^T h(q,\dot{q}) = B^T\tau. \tag{14}$$

Expanding and collecting terms:

$$B^T M B\,\ddot{\theta} + B^T\Big[M(q)\,\dot{B}(q)\,\dot{\theta} + h(q,\dot{q})\Big] = B^T\tau. \tag{15}$$

The effective inertia is defined as

$$I_{eff}(\theta) = B^T M(q)\,B. \tag{16}$$

The nonlinear projection term, grouping Coriolis and gravitational effects, is defined as

$$proj(\theta,\dot{\theta}) = B^T\Big[M(q)\,\dot{B}(q)\,\dot{\theta} + h(q,\dot{q})\Big]. \tag{17}$$

Assuming that only the crank joint is actuated, the final reduced scalar equation of motion becomes

$$I_{eff}(\theta)\,\ddot{\theta} = \tau_m - \tau_{fric} - \tau_{ext} - \tau_{pass} - proj. \tag{18}$$

$$\tau_{\text{fric}} = B^T\Big[b\,\dot{\theta} + f_c\,\tanh\Big(\dot{\theta}/\varepsilon\Big)\Big] \tag{19}$$

$$\tau^{joint}_{pass,i} = B^T\left[k_i(e^{\alpha_i q_i} - 1) + d_i\,\dot{q}_i\right] \tag{20}$$

$$\tau_{ext} = B^T J^T_{ce} f_{ext} \tag{21}$$

VI. Numerical Implementation in ROS 2

A. Execution Pipeline

The reduced dynamic model is implemented in a ROS 2 node. The scalar state $(\theta,\dot{\theta})$ is propagated while the full multibody quantities are evaluated online. At each time step Δt, the following operations are performed:

1) Solve the nonlinear loop-closure problem to obtain a configuration $q(\theta)$ satisfying $\Phi(q) = 0$.
2) Construct the constraint matrix $A(q)$ from the Jacobians of the auxiliary frame pairs.
3) Compute the admissible motion direction $B(q)$ such that $A(q)B(q) = 0$ and $B_\theta = 1$.
4) Approximate $\dot{B}(q)$ using finite differences.
5) Evaluate the inertia matrix $M(q)$ and nonlinear terms $h(q,\dot{q})$ using CRBA and RNEA.
6) Assemble and integrate the reduced scalar dynamic equation.

This procedure preserves consistency with the URDF-based multibody model while avoiding the direct integration of a constrained differential–algebraic system.

B. Constraint Matrix and Projection Vector

For each auxiliary frame pair (A,B) associated with an opened kinematic loop, the translational Jacobians are computed using Pinocchio. Let $J_A(q)$ and $J_B(q)$ denote the corresponding frame Jacobians. The constraint block is

$$A_i(q) = J_A(q) - J_B(q). \tag{22}$$

Stacking all blocks yields the constraint matrix

$$A(q) = \begin{bmatrix} A_1(q) \\ \vdots \\ A_m(q) \end{bmatrix}. \tag{23}$$

The admissible velocity direction satisfies

$$A(q)B(q) = 0. \tag{24}$$

To enforce the crank coordinate as independent variable, the additional condition

$$B_\theta = 1 \tag{25}$$

is imposed. The projection vector is written as

$$B(q) = e_\theta + x, \tag{26}$$

with $x_\theta = 0$. Substituting into (24) gives

$$A_{\text{red}}(q)x_{\text{red}} = -A(q)e_\theta. \tag{27}$$

The solution is obtained in the least–squares sense

$$x_{\text{red}} = \arg\min \|A_{\text{red}}(q)x_{\text{red}} + A(q)e_\theta\|_2^2, \tag{28}$$

yielding the kinematic reduction vector $B(q)$.

C. Numerical Evaluation

The time derivative of the projection vector is approximated through finite differences

$$\dot{B}(q) \approx \frac{B(q_k) - B(q_{k-1})}{\Delta t}. \tag{29}$$

The inertia matrix and nonlinear terms are evaluated using rigid–body dynamics algorithms

$$M(q) = \text{CRBA}(q), \qquad h(q,\dot{q}) = \text{RNEA}(q,\dot{q},0). \tag{30}$$

Finally, the reduced scalar equation

$$I_{\text{eff}}(\theta)\ddot{\theta} = \tau_m - \tau_{fric} - \tau_{ext} - \tau_{pass} - proj \tag{31}$$

is integrated to update the state $(\theta,\dot{\theta})$.

The integration sensitivity was assessed by sweeping $\Delta t \in \{0.1,\, 0.5,\, 1.0,\, 2.0\}$ ms, using $\Delta t = 0.1$ ms as ground truth. At the nominal operating step $\Delta t = 1$ ms, the relative trajectory error on θ is $0.22\,\%$ (RMSE 1.6×10^{-3} rad), while doubling the step to 2 ms increases the error by a factor of 6.3 without inducing divergence. These results indicate that the first-order finite-difference approximation of $\dot{B}(q)$ remains numerically stable and introduces only bounded sub-percent trajectory errors under the considered operating conditions.

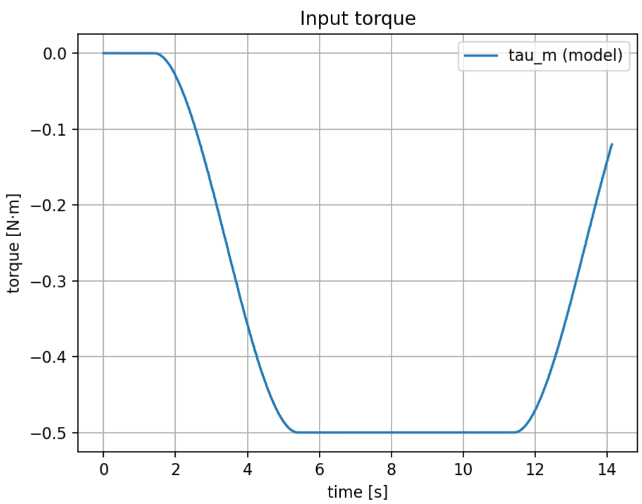

Fig. 2. Applied crank torque profile used to excite the digital twin model

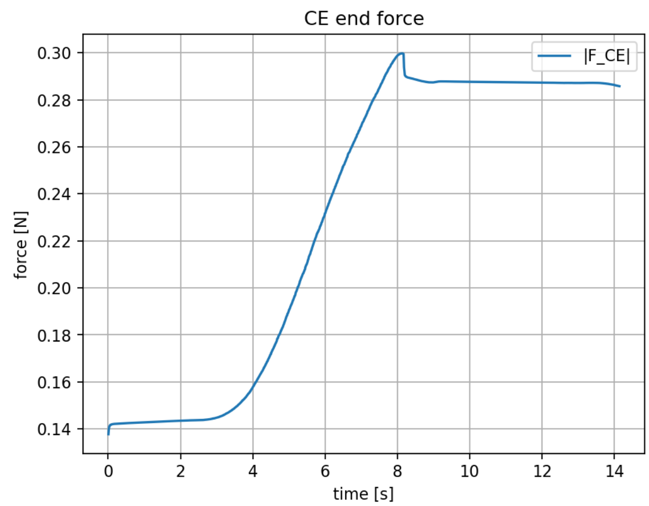

Fig. 3. Predicted end–effector force magnitude during the simulated motion.

VII. Preliminary Results

To assess the behavior of the proposed Digital Twin, a set of preliminary simulations was conducted using the reduced-order dynamic model described in the previous section. Since the physical exoskeleton is currently at a prototype stage, accurate inertial parameters are not yet available. Therefore, the model is instantiated with nominal constant inertial values, and the purpose of these simulations is primarily to evaluate the numerical stability of the modeling framework and the consistency of the constraint reconstruction. These results should be interpreted as preliminary validation of the numerical modeling framework rather than a quantitative evaluation of the physical device. The system is excited by applying a smooth torque profile at the crank joint, shown in Fig. 2. The input follows a ramp–hold–release profile, allowing the mechanism to explore a range of configurations while avoiding abrupt dynamic transients. This excitation enables the reduced dynamic model to be evaluated across the reachable configuration space. Fig. 3 reports the resulting end–effector contact force magnitude during the simulated motion. As the applied torque increases, the predicted force grows smoothly and reaches a peak during the ramp phase. Once the torque input stabilizes, the force response converges to a quasi-steady value. The absence of oscillatory artifacts indicates that the reduced-order dynamic formulation provides numerically stable integration. To further investigate the relationship between mechanism configuration and interaction force, Fig. 4 shows the contact force magnitude as a function of the crank angle. The color map represents the crank angular velocity. The map highlights the nonlinear relationship between configuration and force transmission arising from the mechanism closed-chain kinematics. This behavior reflects the geometry-dependent mechanical advantage of the transmission. Finally, the numerical consistency of the loop-closure reconstruction was evaluated by monitoring the residual norm of the kinematic constraints during the simulation. As shown in Fig. 5, the closure residual remains on the order of 10^{-6} throughout the motion. This result confirms that the nonlinear solver used to reconstruct the closed-chain configuration achieves high numerical accuracy while remaining compatible with standard rigid-body dynamics tools.

The monotonic growth from zero to approximately 5×10^{-6} m does not indicate constraint-violation accumulation. A forward-return sweep confirms that the residual is a deterministic function of θ, arising solely from a minor geometric inconsistency introduced during the CAD-to-URDF conversion rather than numerical drift.

The computational cost was assessed on an Intel Core i7-1065G7. At $\Delta t = 1\,\mathrm{ms}$, the ROS 2 implementation has a mean per-step wall time of $1.31\,\mathrm{ms}$, corresponding to a $1.31\times$ real-time factor. The kinematic closure solver accounts for approximately $85\,\%$ of the total cost, while the

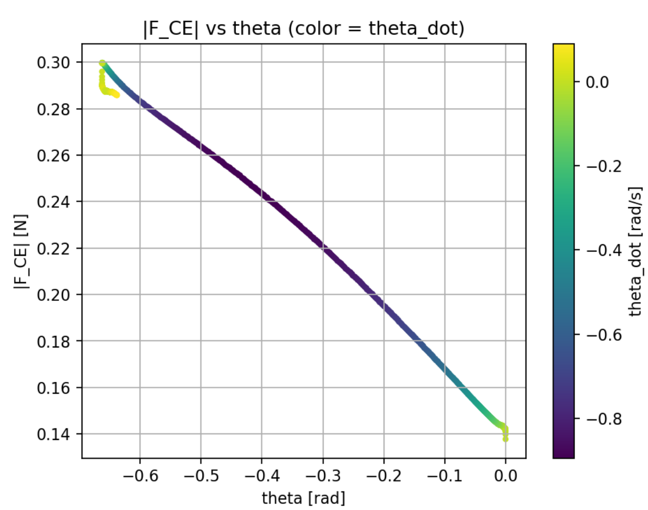

Fig. 4. End–effector force magnitude as a function of the crank angle. The color map represents the crank angular velocity.

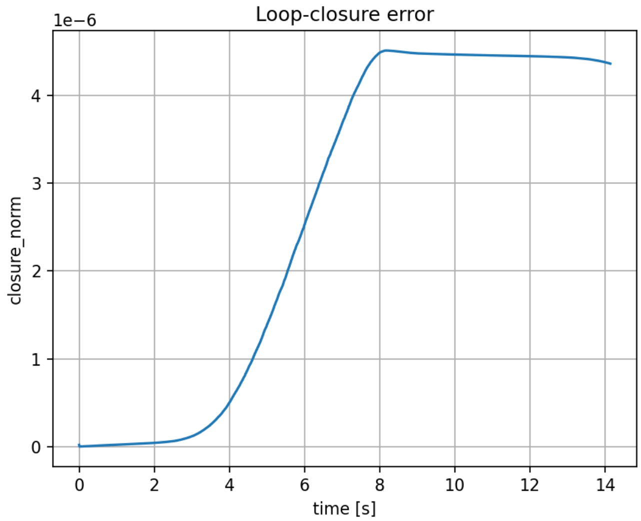

Fig. 5. Loop–closure residual norm during simulation. The constraint error remains within the order of 10^{-6}.

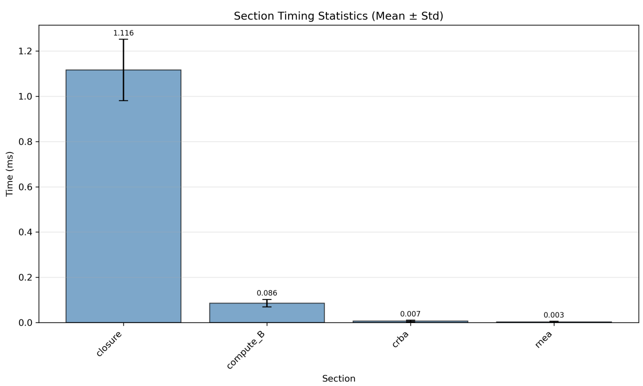

Fig. 6. Per-section breakdown of the mean per-step wall time in the ROS 2 deployment ($\Delta t = 1$ ms, 18 901 steps). The kinematic closure solver dominates at 85 % of total time (1.12 ms); all Pinocchio algebra (CRBA, RNEA, B-vector solve) contributes 0.10 ms combined.

remaining rigid-body algebra is negligible. Increasing Δt to 1.5–2 ms or using a compiled closure solver could support hard real-time operation.

These preliminary results indicate that the proposed Digital Twin framework consistently reproduces the constrained kinematics and configuration-dependent force transmission of the exoskeleton prototype while maintaining numerical stability. This provides a solid basis for future developments, including experimental parameter identification and real-time model-based control.

VIII. Conclusion and Future Work

This work presented a constraint-consistent Digital Twin of a hand exoskeleton implemented within a ROS 2 framework through a CAD-to-URDF modeling pipeline. Closed kinematic chains were handled through numerical loop-closure reconstruction, preserving compatibility with standard rigid-body dynamics libraries. The constrained multibody dynamics was reduced to a scalar nonlinear equation by projecting the joint-space dynamics onto the null space of the constraint Jacobian. This formulation avoids the direct integration of differential–algebraic equations while retaining configuration-dependent inertial redistribution and nonlinear velocity effects, enabling deterministic real-time execution. The proposed Digital Twin models a prototype hand exoskeleton currently under development. Consequently, the present implementation relies on nominal parameters and simplified representations of joint friction and human passive elastic torques. Future work will address system identification of friction coefficients and subject-specific passive biomechanical contributions in order to improve the predictive accuracy of human–exoskeleton interaction. As the hardware architecture becomes fully consolidated and experimental data become available, the Digital Twin will evolve from a verified simulation framework into a calibrated real-time control layer for the physical exoskeleton, supporting torque compensation and constraint-consistent motion generation. From a clinical standpoint, the framework already enables therapists to simulate the expected force–angle profile for planned actuation sequences and adapt control parameters to the patient's anatomy before the rehabilitation session begins.

References

[1] Y. H. Park and D. H. Lee, "Robot-Assisted Treatments for Gait Rehabilitation in Stroke Patients: A Review,"*Medicina*, vol. 60, no. 4, p. 620, 2024.

[2] A. Topini, W. Sansom, N. Secciani, L. Bartalucci, A. Ridolfi, and B. Allotta, "Variable Admittance Control of a Hand Exoskeleton for Virtual Reality-Based Rehabilitation Tasks," *Frontiers in Neurorobotics*, vol. 15, p. 789743, 2022.

[3] B. R. Barricelli, E. Casiraghi, and D. Fogli,"A Survey on Digital Twin: Definitions, Characteristics, Applications, and Design Implications," *IEEE Access*, vol. 7, pp. 167653–167671, 2019.

[4] M. W. Lauer-Schmaltz, P. Cash, J. P. Hansen, and N. Das, "Human Digital Twins in Rehabilitation: A Case Study on Exoskeleton and Serious-Game-Based Stroke Rehabilitation Using the ETHICA Methodology," *IEEE Access*, vol. 12, pp. 180968–180988, 2024.

[5] L. Bartalucci, C. Brogi, A. Bucci, A. Topini, A. Della Valle, N. Secciani, A. Ridolfi, and B. Allotta, "A kinaesthetic hand exoskeleton system toward robot-augmented rehabilitation therapies in the Health 4.0 era," in *Proc. 10th Int. Conf. Bioinformatics Research and Applications (ICBRA)*, New York, NY, USA, 2024, pp. 135–142.

[6] N. Qiu, C. Song, and F. Wan, "Describing robots from design to learning: Towards an interactive lifecycle representation of robots," in *Proc. 2024 Int. Conf. Advanced Robotics and Mechatronics (ICARM)*, pp. 1081–1086, 2024.

[7] J.Carpentier, G.Saurel, G.Buondonno, J.Mirabel, F.Lamiraux, O.Stasse, and N.Mansard, "The Pinocchio C++ library: A fast and flexible implementation of rigid body dynamics algorithms and their analytical derivatives," in *Proc. 2019 IEEE/SICE Int. Symp. System Integration (SII)*, Paris, France, 2019, pp. 614–619, doi: 10.1109/SII.2019.8700380.